# TECHNICAL RESEARCH REPORT

A Spectrally Filtered, Least-Squares Projection Method for Stokes Flow Problems in Driven Cavities

*by Raymond A. Adomaitis*

**T.R. 99-76**

# ISR
**INSTITUTE FOR SYSTEMS RESEARCH**

# A Spectrally Filtered, Least-Squares Projection Method for Stokes Flow Problems in Driven Cavities

Raymond A. Adomaitis

*Department of Chemical Engineering and*

*Institute for Systems Research*

*University of Maryland*

*College Park, MD 20742*

January 7, 1999

**Summary**

A least-squares, weighted residual projection method is presented for computing Stokes flow solutions to driven cavity problems in rectangular and cylindrical geometries. In this procedure, the velocity field components are first defined by eigenfunction expansion solutions to the Stokes flow problem in terms of an unknown pressure field which is subsequently computed by minimizing the continuity equation residual norm by the least-squares projection. The role of spectral filtering methods for improving pointwise solution convergence is also discussed.

**Keywords:** Eigenfunction expansion; driven cavity flows; Stokes flow; convergence; spectral filtering; Gibbs phenomenon.

# 1   Introduction

We consider computing solutions to the Stokes flow problem defined by a cavity filled with liquid set in motion by one cavity wall. This wall is located at $r = 1$ and moves at unit velocity in the axial direction; the remaining walls are stationary (see Fig. 1). Because we assume both velocity components are zero at the stationary walls, an analytical solution in closed form is not possible due to the jump discontinuity of the boundary conditions at both outer corners [4]. This problem has been studied in the context of modeling plasma flow between adjacent red blood cells moving through a capillary blood vessel [5]; other applications include studies of creeping flow eddy structures and their transitions in rectangular cavities by eigenfunction expansion solutions to the stream function formulation of the problem (e.g., [1, 4, 9, 10, 11]). In this paper, we present an alternative to the stream-function based solution approaches: a quadrature-based [6] eigenfunction expansion method is investigated where the pressure field is computed from a least squares projection of the continuity equation residual. We focus on the computational methods and convergence performance of the proposed projection method.

The equations governing the fluid motion are written in dimensionless form as

$$
\begin{aligned}
0 &= -\frac{\partial p}{\partial r} + \frac{\partial}{\partial r}\left( \frac{1}{r^\beta} \frac{\partial}{\partial r}(r^\beta v_r) \right) + \alpha^2 \frac{\partial^2 v_r}{\partial z^2} \\
0 &= -\alpha \frac{\partial p}{\partial z} + \frac{1}{r^\beta} \frac{\partial}{\partial r}\left( r^\beta \frac{\partial v_z}{\partial r} \right) + \alpha^2 \frac{\partial^2 v_z}{\partial z^2}
\end{aligned}
$$

where $\alpha = R/Z$ is the aspect ratio of the cavity and $\beta$ is the geometry factor: $\beta = 0$ for a rectangular cavity with infinite spanwise dimension and $\beta = 1$ for a cylindrical cavity. The continuity condition is

$$
\frac{1}{r^\beta} \frac{\partial}{\partial r}(r^\beta v_r) + \alpha \frac{\partial v_z}{\partial z} = 0.
$$

Boundary conditions are $v_z = 1$ at $r = 1$, $v_z = 0$ at $z = 0, 1$, and $v_r = 0$ at $z = 0, 1$ and $r = 0, 1$. We consider the cases $\partial v_z / \partial r = 0$ for the cylindrical cavity and $v_z = 0$ at $r = 0$ for the rectangular cavity.
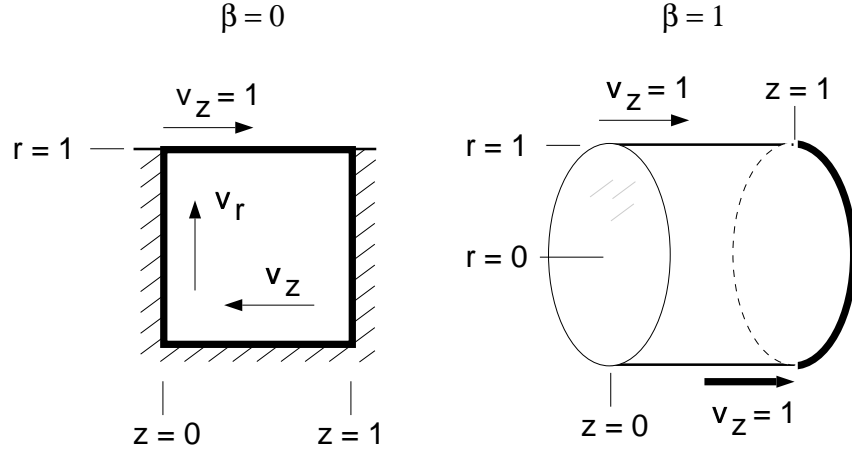
Figure 1: *Flow field geometries.*

## 2   Trial Function Expansions

The fluid velocity components and pressure field are represented by globally-defined trial function expansions of the form

$$
\begin{aligned}
v_r(r, z) &= \sum_{i,j=1}^{M_V} a_{i,j} \phi_i(r) \psi_j(z) \\
v_z(r, z) &= \sum_{i,j=1}^{M_V} b_{i,j} \eta_i(r) \xi_j(z) + \sum_{j=1}^{M_{BC}} c_j r^2 \xi_j(z) \\
p(r, z) &= \sum_{i,j=1}^{M_P} d_{i,j} \gamma_i(r) \delta_j(z)
\end{aligned}
$$

where the trial function components are computed as nontrivial solutions (including nontrivial eigenfunctions associated with zero-value eigenvalues) to the Strum-Liouville problems

$$
\lambda_\phi \phi = \frac{d}{dr} \left( \frac{1}{r^\beta} \frac{d}{dr} (r^\beta \phi) \right) \qquad \lambda_\psi \psi = \frac{d^2 \psi}{dz^2}
$$

$$
\lambda_\eta \eta = \frac{1}{r^\beta} \frac{d}{dr} \left( r^\beta \frac{d\eta}{dr} \right) \qquad \lambda_\xi \xi = \frac{d^2 \xi}{dz^2}
$$

$$
\lambda_\gamma \gamma = \frac{1}{r^\beta} \frac{d}{dr} \left( r^\beta \frac{d\gamma}{dr} \right) \qquad \lambda_\delta \delta = \frac{d^2 \delta}{dz^2}
$$

subject to boundary conditions $\phi(0) = \phi(1) = 0$, $\psi(0) = \psi(1) = 0$, $\eta(1) = 0$, $\xi(0) = \xi(1) = 0$, $\gamma'(0) = \gamma'(1) = 0$, $\delta'(0) = \delta'(1) = 0$, and either $\eta(0) = 0$ (for $\beta = 0$) or $\eta'(0) = 0$ (for $\beta = 1$). We note that while $\psi_i$ and $\xi_i$ are computed from the same Sturm-Liouville problem, only odd functions are used to define the $\psi_i$ and even for $\xi_i$; odd functions are used to define the $\delta_i$. The trial functions are orthogonal sequences (and are normalized) with respect to the inner product

$$
\begin{aligned}
\langle \phi_i \psi_j, \phi_k \psi_l \rangle_{r,z} &= \langle \phi_i, \phi_k \rangle_r \langle \psi_j, \psi_l \rangle_z \\
&= \int_{r=0}^{1} \phi_i(r)\phi_k(r)\, r^\beta dr \int_{z=0}^{1} \psi_j(z)\psi_l(z)\, dz.
\end{aligned}
$$

## 2.1   Flow Velocity Components

Substituting the trial function expansions into the momentum balance equations, we obtain for the radial velocity component $v_r$

$$
\sum_{i,j=1}^{M_P} d_{i,j}\gamma_i'\delta_j = \sum_{i,j=1}^{M_V} a_{i,j}(\lambda_{\phi_i} + \alpha^2 \lambda_{\psi_j})\phi_i\psi_j
$$

where the prime denotes differentiation (with respect to $r$ in this case). Solving for the coefficient $a_{p,q}$ by projecting this residual onto $\phi_p\psi_q$, we obtain

$$
a_{p,q} = \frac{1}{\lambda_{\phi_p} + \alpha^2 \lambda_{\psi_q}} \sum_{i,j=1}^{M_P} \langle \gamma_i'\delta_j, \phi_p\psi_q \rangle_{r,z}\, d_{i,j}.
$$

An important numerical simplification we observe is that $\gamma_i'(r)$ and $\phi_p(r)$ satisfy the same eigenvalue problem. Therefore, $\langle \gamma_i', \phi_p \rangle_r = 0$ for all $i \neq p+1$, and the eigenfunction expansion solution simplifies to

$$
\begin{aligned}
a_{p,q} &= \frac{\langle \gamma_{p+1}', \phi_p \rangle_r}{\lambda_{\phi_p} + \alpha^2 \lambda_{\psi_q}} \sum_{k=1}^{M_P} \langle \delta_k, \psi_q \rangle_z\, d_{p+1,k} \\
&= \sum_{k=1}^{M_P} A_{p,q,k}\, d_{p+1,k}.
\end{aligned}
\tag{1}
$$

As the first step of determining a solution to the axial velocity component $v_z$, we represent the nonhomoge-

neous contribution to this velocity component as

$$v_{z_{\partial \Omega}} = \sum_{j=1}^{M_{BC}} \sigma_j c_j r^2 \xi_j(z) \tag{2}$$

and compute the coefficients $c_j$ by

$$c_j = \langle 1, \xi_j \rangle_z = \int_{z=0}^{1} \xi_j \, dz.$$

The spectral filter constants $\sigma_j$ will be discussed later in this paper. The residual function for the axial

velocity component is

$$\alpha \sum_{i,j=1}^{M_P} d_{i,j} \gamma_i \delta_j' = \sum_{i,j=1}^{M_V} b_{i,j}(\lambda_{\eta_i} + \alpha^2 \lambda_{\xi_j}) \eta_i \xi_j + \nabla^2 v_{z_{\partial \Omega}}$$

with $\nabla^2 v_{z_{\partial \Omega}} = \sum_{j=1}^{M_{BC}} c_j \left[ 2(\beta + 1) + \alpha^2 r^2 \lambda_{\xi_j} \right] \xi_j$. Projecting this function onto $\eta_p \xi_q$ and solving for the $b_{p,q}$

gives

$$b_{p,q} = \frac{\alpha}{\lambda_{\eta_p} + \alpha^2 \lambda_{\xi_q}} \sum_{i,j=1}^{M_P} \langle \gamma_i \delta_j', \eta_p \xi_q \rangle_{r,z} d_{i,j} - \frac{c_q \langle \left[ 2(\beta + 1) + \alpha^2 r^2 \lambda_{\xi_q} \right], \eta_p \rangle_r}{\lambda_{\eta_p} + \alpha^2 \lambda_{\xi_q}}.$$

Similar to the radial component case, the choice of even $\xi_i(z)$ and odd $\delta_j(z)$ means that $\xi_i$ and $\delta_j'$ satisfy the

same eigenvalue problem and that $\langle \xi_i, \delta_j' \rangle_z = 0$ for all $i \neq j$. Therefore,

$$
\begin{aligned}
b_{p,q} &= \frac{\alpha \langle \delta_q', \xi_q \rangle_z}{\lambda_{\eta_p} + \alpha^2 \lambda_{\xi_q}} \sum_{k=1}^{M_P} \langle \gamma_k, \eta_p \rangle_r d_{k,q} - e_{p,q} \\
&= \sum_{k=1}^{M_P} B_{p,q,k} d_{k,q} - e_{p,q}. \tag{3}
\end{aligned}
$$

# 3   The Projection Method

Having effectively written the solutions to both velocity field components in terms of the still unknown

pressure field, we can substitute the coefficient arrays **a** and **b** back into their trial function expansions to

evaluate the velocity field components and substitute these into the continuity equation to determine the

pressure field that satisfies the continuity equation. This gives

$$\sum_{i,j=1}^{M_V} \mathcal{L}\phi_i\psi_j a_{i,j} + \alpha b_{i,j}\eta_i\xi_j' + \alpha\nabla_z v_{z_{\partial\Omega}} = 0$$

where $\nabla_z = \partial/\partial z$ and

$$\mathcal{L}\phi_i = \frac{1}{r^\beta}\frac{d}{dr}r^\beta\phi_i.$$

In terms of the pressure field coefficients $\mathbf{d}$, the residual function can be written as

$$R_c(r,z) = \alpha\nabla_z v_{z_{\partial\Omega}} + \sum_{i,j=1}^{M_V} \mathcal{L}\phi_i\psi_j \sum_{k=1}^{M_P} A_{i,j,k}d_{i+1,k} + \alpha\left[B_{i,j,k}d_{k,j} - e_{i,j}\right]\eta_i\xi_j'. \tag{4}$$

The least-squares projection consists of determining the $d_{p,q}$ that satisfy

$$\left\langle R_c(r,z), \frac{\partial R_c}{\partial d_{p,q}} \right\rangle_{w_r,w_z} = 0 \qquad \text{or} \qquad \left\langle R_c(r,z), T_{p,q} \right\rangle_{w_r,w_z} = 0 \tag{5}$$

for $p,q = 1,\ldots,M_P$, and with test functions $T_{p,q}$ defined by

$$T_{p,q} = \mathcal{L}\phi_{p-1}\sum_{k=1}^{M_V}\psi_k A_{p-1,k,q} + \alpha\xi_q'\sum_{k=1}^{M_V}\eta_k B_{k,q,p}.$$

The projection operation is based on the *weighted* inner product

$$\begin{aligned}
\langle \phi_i\psi_j, \phi_k\psi_l \rangle_{w_r,w_z} &= \langle \phi_i, \phi_k \rangle_{w_r}\langle \psi_j, \psi_l \rangle_{w_z} \\
&= \int_{r=0}^1 \phi_i(r)\phi_k(r)\,w_r(r)\,r^\beta dr \int_{z=0}^1 \psi_j(z)\psi_l(z)\,w_w(w)\,dz.
\end{aligned}$$

For this study, we choose $w_r(r) = (1-r)^2$ and $w_z = (2z-1)^2$ to enhance the corner flow and pressure field convergence. Therefore, if

$$J_{p,q,i,j} = \langle T_{i,j}, T_{p,q} \rangle_{w_r,w_z}$$

$$f_{p,q} \quad = \quad \alpha \sum_{m,n}^{M_V} e_{m,n} \left\langle \eta_m \xi_n', T_{p,q} \right\rangle_{w_r, w_z} - \alpha \sum_{j=1}^{M_{BC}} \sigma_j c_j \left\langle r^2 \xi_j', T_{p,q} \right\rangle_{w_r, w_z}$$

we can determine the pressure field coefficients by solving the $M_P \times M_P$ set of linear equations resulting

from condition (5). The elements of the linear equation coefficient array can be written explicitly as

$$J_{p,q,i,j} \quad = \quad \left\langle \mathcal{L}\phi_{i-1}, \mathcal{L}\phi_{p-1} \right\rangle_{w_r} \sum_{k,l=1}^{M_V} \left\langle \psi_k, \psi_l \right\rangle_{w_r} A_{i-1,l,j} A_{p-1,k,q} + \alpha \sum_{k=1}^{M_V} \left\langle \mathcal{L}\phi_{i-1}, \eta_k \right\rangle_{w_r} B_{k,q,p} \sum_{l=1}^{M_V} \left\langle \psi_l, \xi_q' \right\rangle_{w_z} A_{i-1,l,j}$$

$$+ \alpha \sum_{l=1}^{M_V} \left\langle \mathcal{L}\phi_{p-1}, \eta_l \right\rangle_{w_r} B_{l,j,i} \sum_{k=1}^{M_V} \left\langle \psi_k, \xi_j' \right\rangle_{w_z} A_{p-1,k,q} + \alpha^2 \left\langle \xi_j', \xi_q' \right\rangle_{w_z} \sum_{k,l=1}^{M_V} \left\langle \eta_k, \eta_l \right\rangle_{w_r} B_{l,j,i} B_{k,q,p}$$

and the nonhomogeneous terms as

$$f_{p,q} \quad = \quad \alpha \sum_{k,m,n=1}^{M_V} \left\langle \mathcal{L}\phi_{p-1}, \eta_m \right\rangle_{w_r} \left\langle \psi_k, \xi_n' \right\rangle_{w_z} e_{m,n} A_{p-1,k,q} + \alpha^2 \sum_{m,n=1}^{M_V} e_{m,n} \left\langle \xi_q', \xi_n' \right\rangle_{w_z} \sum_{k=1}^{M_V} B_{k,q,p} \left\langle \eta_k, \eta_m \right\rangle_{w_r}$$

$$- \alpha \sum_{j=1}^{M_{BC}} \sigma_j c_j \left\langle \mathcal{L}\phi_{p-1}, r^2 \right\rangle_{w_r} \sum_{k=1}^{M_V} \left\langle \psi_k, \xi_j' \right\rangle_{w_z} A_{p-1,k,q} - \alpha^2 \sum_{j=1}^{M_{BC}} \sigma_j c_j \left\langle \xi_q', \xi_j' \right\rangle_{w_z} \sum_{k=1}^{M_V} B_{k,q,p} \left\langle \eta_k, r^2 \right\rangle_{w_r}.$$

The system of linear equations $\mathbf{Jd} = \mathbf{f}$ resulting from the least-squares projection is solved by first re-indexing

the equations and pressure field mode amplitude coefficients $\mathbf{d}$ and then solving the $M_P^2 \times M_P^2$ set of linear

equations. We note that because there is no "flat" mode in the pressure field trial function expansion, the

solution has a zero-mean pressure field. We call this $M_P \times M_P$ array of coefficients $\mathbf{d}_{M_P}$.

The weighted inner products defining the coefficients $J_{p,q,i,j}$ are computed with a numerical procedure

based on discrete approximations to the eigenfunctions, represented in discretized form by their values at

Gauss-Lobatto quadrature points. Accurate discrete differentiation operations (to be used for computing the

residual function $R_c$) are formulated by representing the eigenfunctions in terms of Lagrangian interpolation

functions [6]. We find that computing the weighted inner products using $N = 4M_V$ quadrature points to be

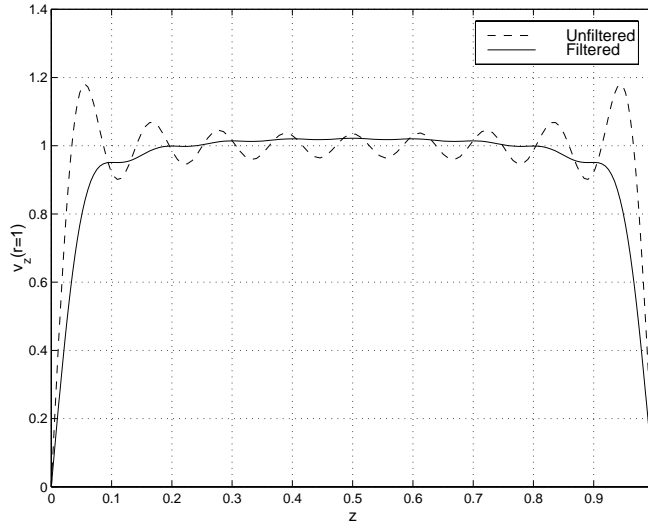sufficiently accurate and not computationally intensive.

Figure 2: *Spectrally-filtered and direct projections of the axial velocity component profile at the outer wall* $(r = 1)$ *for* $M_{BC} = 9$.

# 4   Spectral Filtering

Because of the velocity field boundary condition jump discontinuities at the corners $r = 1$, $z = 0, 1$, global spectral filtering techniques are used to smooth the Gibbs oscillations ([2] and see Fig. 2). In Fig. 2, we compare $v_{z_{\partial\Omega}}$ computed from a direct projection of the nonhomogeneous boundary condition to the velocity profile reconstructed using filter coefficients that give the equivalent to the Cesaro sums [4, 8] of (2), where

$$\sigma_j = 1 - \frac{j-1}{M_{BC}} \qquad j = 1, \ldots, M_{BC}.$$

The filtered projection is significantly smoother than the direct projection and was necessary for obtaining converged solutions. Other spectral filtering methods will also work; an overview of these methods can be found in [3].

If the residual function $R_c(r, z)$ (4) is computed for two successive values of $M_P$, we find that the functions in the neighborhood of the corner points $r = 0$ and $z = 0, 1$ have approximately zero mean but are of opposite sign. This suggests that filtering can also be used to reduce the residual magnitude in these regions without sacrificing convergence in the remaining physical domain. We implement this filtering methodology

by computing the Cesaro sums of a sequence of solutions $\mathbf{d}_M$ to obtain the filtered pressure field profile $\bar{\mathbf{d}}_{M_P}$:

$$\bar{\mathbf{d}}_{M_P} = \frac{1}{M_P - M_{BC} + 1} \sum_{M=M_{BC}}^{M_P} \mathbf{d}_M.$$

The axial and radial velocity components are then computed from the filtered pressure field using (3) and (1), respectively. A representative solution is shown in Fig. 3 for the case of $\alpha = 1$ and $\beta = 0$; results for $\beta = 1$ and other values of the aspect ratio $\alpha$ will be discussed in a subsequent paper.

# 5   Convergence

Convergence of the computed solutions can be quantified as a function of truncation number in terms of the $L^2$ norm of the continuity equation residual function $\|R_c\| = \sqrt{\langle R_c, R_c \rangle_{r,z}}$, a quantity easily computed using the discrete differentiation operations and quadrature techniques discussed previously. If the truncation number of the trial function expansion defining the nonhomogeneous contribution to the axial velocity component (2) is increased at the same rate as the overall solution truncation number ($M_{BC} = M_P$), the axial velocity component gradient will grow infinitely large as $M_P$ grows. This would ultimately (as $M_P \to \infty$) lead to infinite static pressure in the corners, a result consistent with the similarity solutions of Moffatt [7], resulting in a divergent sequence of solution norms. To obtain convergent solution sequences, we consider cases where $M_{BC}$ is fixed and convergence is studied in terms of solution truncation number $M_P$; under these circumstances, we find the residual norms diminish with increasing $M_P$.

Another means of assessing computed solution accuracy is to evaluate the stream function $\Psi(r, z)$, defined for the two geometries considered in this paper as

$$v_r = \frac{\alpha}{r^\beta} \frac{\partial \Psi}{\partial z} \qquad v_z = -\frac{1}{r^\beta} \frac{\partial \Psi}{\partial r}.$$

For the case $\beta = 0$, we can compute the stream function explicitly because the trial function components are $\psi_q(z) = \sqrt{2} \sin 2q\pi z$ and $\eta_p(r) = \sqrt{2} \sin \pi pr$. The stream functions can be computed from the velocity
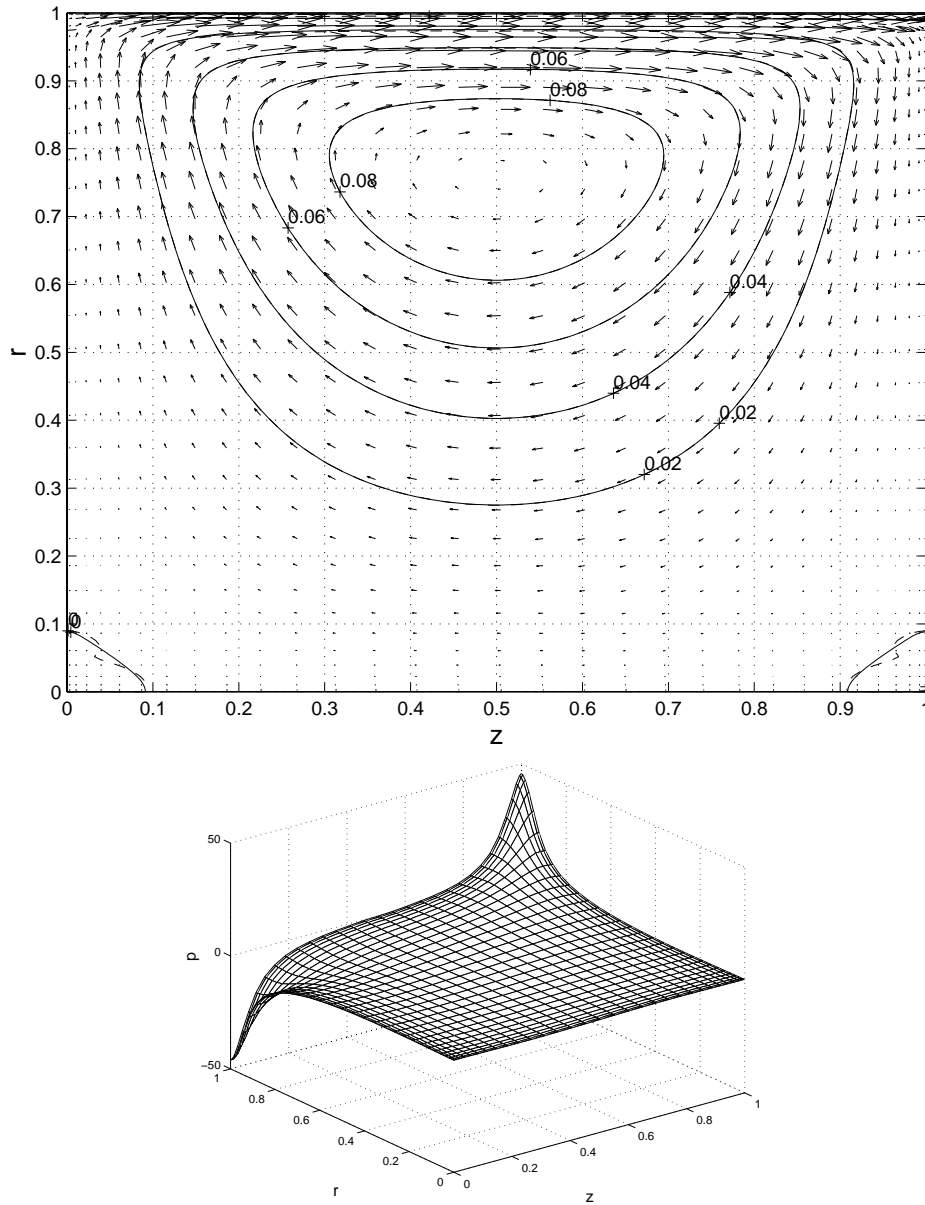
Figure 3: *Stream function contours* $\Psi_{(r)}$ *(solid) and* $\Psi_{(z)}$ *(dashed), and velocity components (top), and the static pressure field (bottom) for* $M_P = 25$, $M_V = 40$, $M_{BC} = 9$, $\alpha = 1$, *and* $\beta = 0$.

field component trial function expansions for $v_r$ and $v_z$ as

$$
\begin{aligned}
\Psi_{(r)}(r, z) &= \sum_{p,q=1}^{M_V} \frac{\sqrt{2}}{2\alpha q\pi} a_{p,q} \phi_p(r) \left[1 - \cos 2q\pi z\right] \\
\Psi_{(z)}(r, z) &= -\sum_{p,q=1}^{M_V} \frac{\sqrt{2}}{\pi p} b_{p,q} \left[1 - \cos \pi pr\right] \xi_q(z) - \sum_{j=1}^{M_{BC}} \frac{\sigma_j c_j}{3} r^3 \xi_j(z)
\end{aligned}
$$

respectively. The overall accuracy of the computed solution can then be gauged by comparing the two stream functions. As can be seen in Fig. 3, the larger-scale structures emerge first and the smaller-scale corner eddies develop with increasing $M_P$. These observations are consistent with physical intuition and the convergence properties of global spectral methods. In this Figure, we observe small deviations in the two stream functions in the neighborhood of the corner eddies (the streamlines of the large eddy overlap in this Figure). The differences in the corner eddy streamfunction structures diminish with increasing $M_P$.

# 6   Conclusions

In this paper, we presented an alternative to the stream-function based solution approaches to Stokes flow problems in driven cavities, where the pressure field is computed directly from a least squares projection of the continuity equation residual. Explicit descriptions of the numerical procedure were given for two cavity geometries. The convergence performance of the projection method was discussed in terms of the spectral filtering methods necessary for improved pointwise convergence of the velocity and pressure fields.

The results presented in this paper demonstrate that accurate solutions to the large-eddy structure can be obtained with a moderate number of modes, with increased resolution possible with increasing truncation number. Subsequent studies will focus on eddy structure transitions as a function of aspect ratio for the two geometry factors. We see this approach as being directly applicable to three-dimensional flows and other cavity geometries.

## Acknowledgments

## References

[1] Burggraf, O. R., 'Analytical and numerical studies of the structure of steady separated flows', *J. Fluid Mech.* **24** 113-151 (1966).

[2] Gottlieb, D. and S. A. Orszag, *Numerical Analysis of Spectral Methods* SIAM CBMS-NSF Regional Conf. Series in Appl. Math. Vol. 26, 1977.

[3] Gottlieb, D. and C. -W. Shu, 'On the Gibbs phenomenon and its resolution', *SIAM Rev.* **39** 644-668 (1997).

[4] Joseph, D. D. and L. Sturges, 'The convergence of biorthogonal series for biharmonic and Stokes flow edge problems: part II', *SIAM J. Appl. Math.* **34** 7-26 (1978).

[5] Lew, H. S. and Y. C. Fung, 'The motion of the plasma between the red blood cells in bolus flow', *Biorheology* **6** 109-119 (1969).

[6] Lin, Y. -h., Chang, H. -Y., and R. A. Adomaitis, 'MWRtools: A library for weighted residual methods', *ISR TR 98-24* (1998).

[7] Moffatt, H. K., 'Viscous and resistive eddies near a sharp corner', *J. Fluid Mech.* **18** 1-18 (1964).

[8] Navarra, A., W. F. Stern, and K. Miyakoda, 'Reduction of the Gibbs oscillation in spectral model simulations', *J. Climate* **7** 1169-1183 (1994).

[9] Pan, F. and A. Acrivos, 'Steady flows in rectangular cavities', *J. Fluid Mech.* **28** 643-655 (1967).

[10] Shankar, P. N., 'The eddy structure in Stokes flow in a cavity', *J. Fluid Mech.* **250** 371-383 (1993).

[11] Srinivasan, R., 'Accurate solutions for steady plane flow in the driven cavity. I. Stokes flow', *ZAMP* **46** 524-545 (1995).